INTEGRATION OF HYDROGEN PRODUCTION WITH GEOTHERMAL POWER PLANTS: UTILIZING H2 AS A SPINNING RESERVE UNIT

Alessia Manfredi[1]*, Giampaolo Manfrida[2], Carlo Carcasci[2], Daniele Fiaschi[2]

[1]University of Padova, Department of Industrial Engineering, Padova, Italy

[2] University of Florence, Department of Industrial Engineering, Florence, Italy

*Corresponding Author: alessia.manfredi.1@phd.unipd.it

ABSTRACT

The targeted integration of a Hydrogen-Oxygen direct combustor followed by a high-pressure turbine within an existing geothermal power plant (GPP) is investigated. Hydrogen and Oxygen are produced by an electrolyzer when electricity production form PV is relevant; extra power is produced at night when the demand is high and the cost of electricity higher. This solution uses largely existing equipment in the GPP and represents an alternative for daily energy storage and load shifting with respect to the adoption of dedicated units like batteries. The system can be an alternative to using the electrolyzer coupled to a dedicated fuel cell unit. Thermodynamic and exergy models for each operating mode (accumulation and peak load operation), complemented by economic analyses, provide a multifaceted evaluation. Referring to a standard 20 MWe GPP unit, the peak load capacity is extended 1.4 MWe. The first law efficiency of the integrated system improves to 23.0% with the direct combustor and 24. 9% with the fuel cell, compared to the base plant efficiency of 22.8%. The exergy efficiency shows a slight reduction to 55.04% for the direct combustor mode and 57.5% for the fuel cell mode, from the plant's 58.0%. Economic analysis suggests that the proposed system can potentially offer a cost-effective solution with competitive operational costs. These findings unveil promising prospects, indicating the potential contribution to a more sustainable economic framework.

1 INTRODUCTION

Climate change, driven primarily by the combustion of fossil fuels with the associated greenhouse gas emissions, necessitates a shift towards sustainable energy sources. This change of paradigm will require considerable development of renewable technologies with lower environmental impact. While renewable energy sources offer promising alternatives, their intermittent nature poses a challenge that requires innovative solutions. Geothermal energy represents a major asset in this direction. The use of renewable energy is presently hindered by the stochastic nature of Variable Renewable Energies (VREs), like solar photovoltaics and wind. GPPs provide the fundamental baseload power supply and represent an alternative to fossil fuels like coal or nuclear power, which are typically employed for this purpose. The recent EU Geothermal SRIA (ETIP Geothermal, 2023) stresses this point of attractiveness of geothermal energy, which, besides substituting fossil fuel resources, represents an alternative to the deployment of large-scale energy storage. Compared to the current power production practice, this represents an expensive alternative, and implies drawbacks in terms of sustainability (e.g., end of life of batteries, risks connected to large chemical energy storage,..). Where hydrothermal resources are present, geothermal energy is able to reach substantial power production levels (nearly 1000 MWe in Italy and Kenya; and about 3000 MWe in Turkey), which are currently beyond the potential of biomass; the development of artificial Engineered Geothermal Systems (EGS) should allow geothermal energy to find much broader diffusion.

In many countries, the increasing availability of VREs is driving the market for electricity to determine low prices when there is high production: this is, for example, the situation in Italy, where about 30000

https://doi.org/10.52202/077185-0123

MWe of PV have been installed. Solar energy is relatively predictable in the day-after electricity market, and this determines a low price when radiation is high; on the other hand, the cost of electricity becomes large in the late evening. Considering this situation, it would make sense to reduce the power production of geothermal power plants at noon and possibly increase it at night. However, this load modulation is not easily practicable: in fact, the geothermal reservoir would undergo cyclic stimulation, and the wells themselves are typically operated at a preset flow rate and pressure; moreover, plants are equipped with emissions treatment, which is difficult to adjust under variable flowrate operation.

This situation has suggested to couple electrolyzer technology to GPPs (Karayel et al. 2022; Cao et al., 2020). The electrolyzer, typically a large alkaline unit, accumulates Hydrogen during daytime operation, which is stored in high-pressure vessels for later use; fuel cells are proposed to provide the peak load power when it is needed at night. The electrolyzer and the GPP are in general weakly connected in terms of process integration: the geothermal resource is able to provide some useful preheating, and of course the availability of the water needed for the electrolyzer. In general, no use is mentioned of the oxygen stream, which is also produced in the electrolyzer.

The use of direct combustion of hydrogen with oxygen represents an alternative with respect to the use of fuel cells to produce peak load power. The combustor can directly produce steam at high pressure and temperature, which can be directly expanded in a steam turbine to provide peak load power. This solution has been subject of research since the pilot experiences derived from liquid fuel rocket engine technology (Malyshenko et al., 2004; Sternfeld, 1995). The aerospace propulsion technology (with conditions reduced to acceptable steam power plant technology, using a cooling stream of water/steam within the combustor which is mixed to the combustion products) is attractive because of the very fast possible operation: full load can be reached within 10 s (Dunikov et al., 2022), which is very appreciated for grid ramp-in and frequency control. The preliminary studies demonstrated the possibility of producing a combustor unit of 25-70 MWt, producing steam at pressures in the range 20-40 bar and temperatures up to 515 °C. Stathopoulos et al. (2017) have proposed different solution for integration of a direct H_2-O_2 combustor in existing large steam power plants, showing the possibility of an increase of power output (up to 19 Mwe over the nominal capacity of 480 MWe), with a marginal efficiency for the H_2 peak load extra power over 0,65. Dunikov (2018) presents a study of integration of the H_2-O_2 combustor to an existing double-flash 50 MWe GPP: in this study, it is proposed to operate the plant at 60% reduced power output feeding an electrolyzer at night. During the day, extra steam generation (superheated conditions at about 140-160°C) is produced by direct H_2-O_2 combustion at the low pressure of the second flash (90 -200 kPa), with an expected extra power output of 0,5 to 0,9 MWe.

This study navigates this paradigm shift by examining a single-flash GPP designed for uninterrupted energy supply. The proposed integration of direct hydrogen combustion within an existing geothermal power plant offers a versatile solution to complement PV peak loads, particularly in mediterranean regions, where abundant PV electricity production occurs during the day in summer. The Geothermal Power plant already includes power components which are reliable and tolerate substantial off-design conditions: notably, the turbine and condenser which represent major power plant equipment. In Italian GPPs, a standard design of steam turbines is practiced since over 30 years, with reference sizes (nominally 20 and 60 MWe) which are adapted to different operating pressures and flow rates substituting the blade equipment in the multi-stage turbine. Condensers are of the direct spray type and are adaptable adjusting the coolant spray flow rate. The electric generator can be refurbished in order to boost its power output. These already existing major components of the power plant can be connected to a Hydrogen-Oxygen combustor and to a small high-pressure turbine. The competitiveness of this system with respect to the installation of a dedicated large fuel cell unit for the production of power at night is investigated through exergy and economic analyses. Operating in two modes – storage and power production – the integration of a hydrogen spinning reserve strategically mitigates load fluctuations in photovoltaic energy. This represents a versatile solution surpassing the limitations of conventional storage technologies. Through thermodynamic, economic, and comparative analyses, this study evaluates the system's adaptability under different operational scenarios, highlighting its potential to contribute to a more sustainable energy framework. Acknowledging existing challenges, this research emphasizes the role of hydrogen as a sustainable spinning reserve, supporting the ongoing transition to renewable energy and improved environmental management.

https://doi.org/10.52202/077185-0123

2 POWER PLANTS DESCRIPTIONS

2.1 Base Case Power Plant (BPP)

The GPP here considered (Figure 1) is a single-flash type (DiPippo, 2012), with operating parameters taken from the Bagnore 3 facility, owned by Enel Green Power, located in the Mount Amiata geothermal district. Table 1 provides a synthetic overview of the main parameters characterizing the single flash geothermal unit.

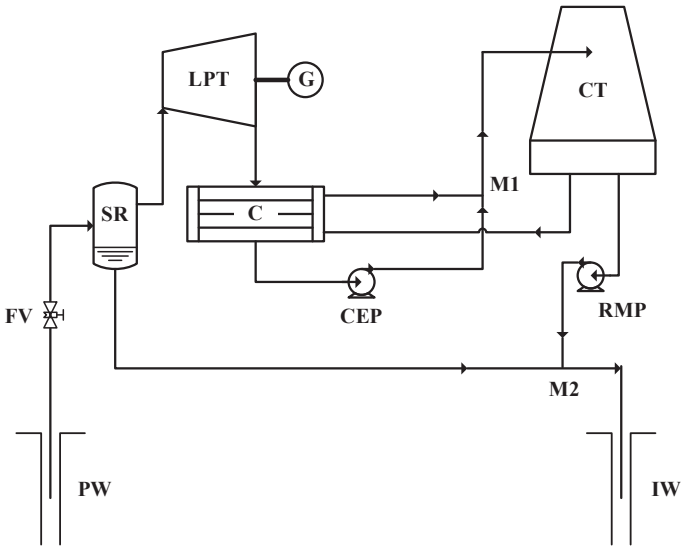

Figure 1: Simplified scheme of a Single Flash Geothermal Power Plant (PW=Production Well, FV=Flash Valve, SR=Separator, LPT=Low Pressure Turbine, SC=Steam Condenser, CEP=Condensate Extraction Pump, CT=Cooling Tower, RMP=Reinjection Mixing Pump, M1=Mixing Point 1, M2=Mixing Point 2)

Table 1: Key reference parameters

Parameter	Unit	Value
Resource Temperature	°C	325
Resource Pressure	bar	250
Pressure at separator	bar	18
Steam flow	t/h	130
Turbine outlet pressure	bar	0.08
Turbine efficiency	%	78.55
Pumps efficiency	%	70
Non-condensable gases	%	8

2.2 Modified Power Plant

The analysis explores integrating an Alkaline Water Electrolyser (AWE) in the base power plant for hydrogen (H_2) and oxygen (O_2) production, storing them for use in an H_2-based spinning reserve unit. Two energy production options are considered: #1: oxy-combustion, with the resulting steam powering turbines, and #2: use in a Proton Exchange Membrane Fuel Cell (PEMFC) for direct electrical generation. The modified plant is operated in two modes: the Accumulation Mode (AM) includes H_2/O_2 production and storage (with decreased power production), while the Booster Mode – (BM) generates extra power with respect to the base plant. The system is designed as a Power-to-Power system, using H_2 to follow the daily electricity demand. The primary goal is using hydrogen as a spinning reserve: during PV production, the system accumulates H_2/O_2; in hours without PV input, it switches to electricity production.

https://doi.org/10.52202/077185-0123

The Accumulation Mode (AM) uses the storage system, identified in Figure 2 by blue lines. This includes an electrolyzer (AWE), pre-cooler (PC), compressors (C) with intercoolers (IC), and the H_2/O_2 storage tanks. The electrolyzer produces 800 Nm^3/h of hydrogen through alkaline electrolysis at 30 bar and 85°C, consuming 4.5 kWh/Nm^3 (Gallandat et al., 2017). The electrolyzer is powered by the low-pressure turbine. The tower drain (condensed steam with low salts content compared to the geothermal brine) is preheated to around 85°C by the flash drain through a heat exchanger (PH). H_2 is compressed at 500 bar and O_2 at 100 bar using intercooled compressors. Three stages of compression are used for H_2, with progressive compressor activation as the pressure in the vessel is raising (variable configuration). After each-compression, the fluid is cooled to 35°C, ensuring thus an isothermal filling process. The initial tank pressure is 10% more than the value needed for the next booster phase (35.2 bar for BM-CC and 1.1 bar for BM-FC). Equation (1) describes the mass storage process.

$$m(t) = m_i + \int_i^t \dot{m} dt \quad (1)$$

In the Booster Mode (BM), the electrolyzer is inactive. In the first scenario (BM-CC), shown in Figure 2 with red lines, H_2 and O_2 are directed from storage to the combustion chamber. Here, some water sent to the cooling tower converges to maintain the chamber's internal temperature after mixing at 540°C. The resulting steam flow rate is first expanded in the high-pressure turbine (HPT); after this, it is mixed (M3) with the geothermal separator stream and directed to the low-pressure turbine (LPT). In the second scenario (BM-FC), illustrated in Figure 2 with green lines, the H_2 and O_2 streams are directed to the PEM fuel cell system for direct electrical energy production. The study applies the performance characteristics of the PEMFC from Campanari et al. (2019). The analysis assumes comparing the two systems with equal electrical production in BM. Therefore, in calculating the input and output flows of the PEMFC, the net efficiency of 49.5%, in line with literature (FCH JU, 2014), is taken into account. To maintain H_2 and O_2 at the required inlet temperature (about 50°C), electric heating with a 10 kW heat duty is applied. Key parameter values are listed in Table 2.

Table 2: Assumed design input data.

AM

Parameter	*Unit*	*Value*
H_2 volumetric flow rate	Nm^3/h	800
AWE pressure	bar	30
AWE temperature	°C	85
AWE energy consumption	kWh/Nm^3	4.5
Coolers water inlet temperature	°C	25
Coolers temperature difference	°C	10
Compressor isentropic efficiency	%	75
Tank volume	m^3	3
Number of H_2 tanks	-	14
Number of O_2 tanks	-	37
Storage H_2 pressure	bar	500
Storage O_2 pressure	bar	100
Initial tank pressure (CC)	bar	35.2
Initial tank pressure (FC)	bar	1.11
Tanks temperature	°C	25

BM-CC

Parameter	*Unit*	*Value*
CC pressure	bar	32
CC temperature	°C	540

BM-FC

Parameter	*Unit*	*Value*
PEMFC pressure	bar	1
Efficiency (net)	%	49.5
FC inlet temperature	°C	50
FC outlet temperature	°C	65

https://doi.org/10.52202/077185-0123

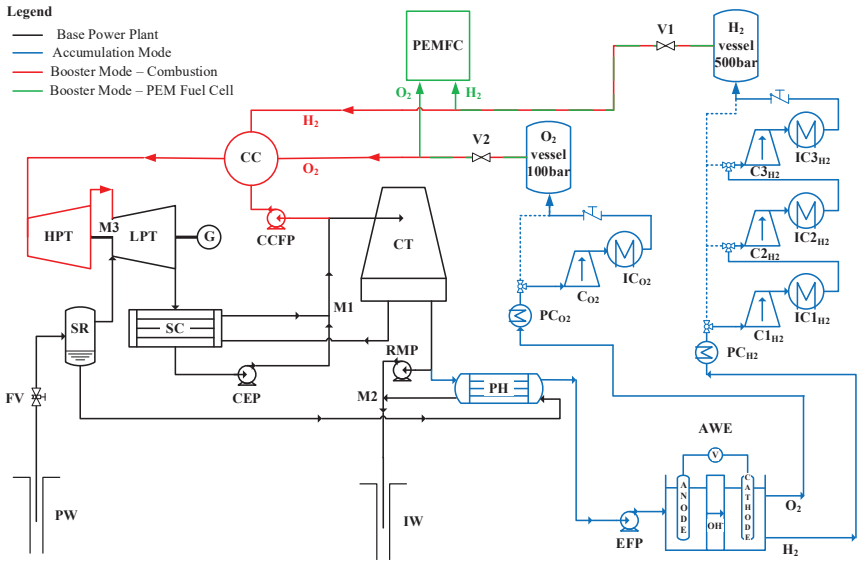

Figure 2: Integrated system schematic with geothermal base plant (black), H_2/O_2 production and storage (blue), combustion-based energy production (red), and PEMFC-based energy production (green). EFP=Electrolyzer Fedwater Pump, CCFP=Combustion Chamber Feedwater Pump.

3 METHODS OF ANALYSIS

3.1 Modeling Approach

To conduct the study, thermodynamic, exergy, and exergo-economic analyses were performed using two distinct models (one for the H_2/O_2 accumulation mode and another for the power production mode). The models were developed using the EES software. Filling and emptying processes of the tanks were modelled under transient conditions. The reference environment model used had properties set at temperature T_0= 25°C, pressure p_0= 101,3 kPa. In the exergy analysis, the real fluid working fluids properties were aligned with JANAF tables to model chemical conditions.

A three-month simulation (May, June, July) is performed, leveraging 2023 hourly time series sourced from Terna S.p.A. for the national Italian photovoltaic production and the Italian market operator GME ("Gestore Mercato Elettrico") for the cost of electricity. The daily electricity demand fluctuates, with PV energy peaks during daylight hours, while geothermal energy maintains near-constant output. The typical day of each month, calculated as the monthly average, was considered. The national PV contribution determines the activation of AM and BM: the first one activates with positive PV contribution, while the second one activates when PV contribution is zero. In June, AM operates for 16 hours/day, while in May and July for 15 hours/day. The BM period consists of the remaining hours of each day.

3.2 Exergy analysis

The exergy analysis follows the guidelines of reference texts (Kotas, 1995; Bejan et al., 1996). A component-level approach is necessary for the following application of Exergo-Economics (EEA) (Meyer et al., 2009), enabling calculation of exergy destructions, losses, efficiency, and destruction ratio for each component. Fuels and Products are defined at the level of the k-th component (Lazzaretto & Tsatsaronis, 2006) so that an exergy balance can be expressed as follows (Eq. (2)):

$$\dot{E}x_{F,k} = \dot{E}x_{P,k} + \dot{E}x_{D,k} + \dot{E}x_{L,k} \quad (2)$$

Furthermore, key exergy performance parameters indicating the system's performance are calculated, including the exergy destruction ratio (Eq. (3)) and the overall exergy efficiency of the system (Eq. (4)), which can be cross-verified by an indirect approach (Eq. (5) which considers the exergy destructions and losses in all the components of the plant.

https://doi.org/10.52202/077185-0123

$$y_k = \frac{\dot{E}x_{D,k}}{\dot{E}x_{F,S}} \quad (3)$$

$$\varepsilon_d = \frac{\dot{E}x_{P,S}}{\dot{E}x_{F,S}} \quad (4)$$

$$\varepsilon_{ind} = 1 - \frac{\sum \dot{E}x_{D,k} + \sum \dot{E}x_{L,k}}{\dot{E}x_{F,S}} \quad (5)$$

3.3 Economic analysis

Cost correlations are applied to obtain the investment, operation, and maintenance (O&M) cost of each component (Turton et al., 2017), with specific adjustment for the geothermal energy systems domain. The annual investment cost of the k-th component is computed at a 10% interest rate over a 20-year lifespan. Equipment costs were updated to the reference year using the CEPCI inflation index (Turton et al., 2017). As proposed by Schuster et al. (2009) and Fiaschi et al. (2017), the O&M cost for each component was defined as 1.5% of the Purchased Equipment Costs (PECs). The yearly plant's operational time for a GPP plant were assumed to be 7446 h/yr (Shokati et al., 2015). The cost correlations were applied to evaluate the Purchased Equipment Costs (PECs), which were sized based on their maximum capacity.

3.4 Exergo-Economic analysis

The primary objective of the exergo-economic analysis (Bejan et al., 1996) is not only to determine the product costs, but also to understand the cost build-up process during energy transformation and its depreciation, described by the progressive decrease of exergy. The cost of the fluid streams along the plant is therefore calculated for each of the 3 months (from May to July) considered in 2023. The EEA of the k-th component involves evaluating equations derived from the balance of input and output costs (Eq. (6)). For systems with N exergy streams exiting the k-th component, N-1 auxiliary equations must be formulated and coupled to the system of cost balance equations, employing the SPECO methodology defined by Lazzaretto & Tsatsaronis (2006). Exergy losses are considered to be priceless during the solution of the system of equations (6). However, following the system's resolution, the cost of destruction or losses for each component can be estimated by pricing it as the cost of the fuel (Eq. 7). The key performance indicator f_k (Eq. 8) identifies the relevance of the investment cost of the k-th component with the sum of the costs of exergy destruction and investment. Another relevant parameter is the product/fuel relative cost increase across the k-th component, r_k (Eq. 9). A complete description of this methodological approach applied to GPPs can be found in Manfrida et al. (2023).

$$\sum_{output}(c_P \dot{E}x_P)_k = \sum_{input}(c_F \dot{E}x_F)_k + \dot{Z}_k \quad (6)$$

$$\dot{C}_{D,k} = c_{D,k}\dot{E}x_{D,k} = c_{F,k}\dot{E}x_{F,k} \quad (7)$$

$$f_k = \frac{\dot{Z}_k}{\dot{Z}_k + \dot{C}_{D,k}} \quad (8)$$

$$r_k = \frac{c_{P,k} - c_{F,k}}{c_{F,k}} \quad (9)$$

4 RESULTS AND DISCUSSION

In the following sections, the results of the thermodynamic, exergy, and exergo-economic analyses are presented. Specifically, the focus is on illustrating the outcomes derived from the situation of maximum power in BM, occurring in June, with a comparison between the base plant and the alternative BP operation modes. Subsequently, a comparative analysis of results across the three considered months is conducted.

https://doi.org/10.52202/077185-0123

4.1 Thermodynamic analysis

The pressure histories in the H_2/O_2 tanks (Figure 3, on the left) highlight differences in the initial tanks pressure between the CC and FC scenarios. The CC model operates with a tank pressure of 35.2 bar, while the FC case begins with a lower pressure of 1.1 bar. With constant H_2 and O_2 flow rates from the AWE, the total stored mass in both scenarios amounts to about 1150 kg of H_2 and 9289 kg of O_2. During emptying of the tanks in BM, in the CC case, the outflow rate is determined by the 8-hour duration of the booster mode cycle (for June). This results in an outflow rate of 0.04 kg/s of H_2 and 0.3 kg/s of O_2, causing the tank pressure to return to its initial cycle value. Conversely, in the FC scenario, the outflow rate is fixed based on the fuel cell efficiency, at 0.02 kg/s of H_2 and 0.18 kg/s of O_2, maintaining an 8-hour emptying process. Consequently, the tank pressure at the end of the emptying process exceeds the initial accumulation cycle value (152.8 bar for H_2 and 26.92 bar for O_2). Therefore, the FC scenario leaves a surplus, resulting in an excess of 473.8 kg of H_2 and 3760.2 kg of O_2 at the cycle's end, which can be sold or used for other purposes. In Figure 3 on the right, the different compressor work in the two scenarios is illustrated. In the FC case, the compressor remains inactive until 1:45 a.m. for H_2, while for O_2, it activates after 7:45 a.m., because of the quite low pressure to be reached for the storage. In the CC case, compressors activate immediately for both fluids, as the tank pressure is already higher than the outlet pressure from the electrolyser. Consequently, in the CC case, total compressor work integral for filling amounts to 1456.6 kWh, compared to 1115.98 kWh in the FC case.

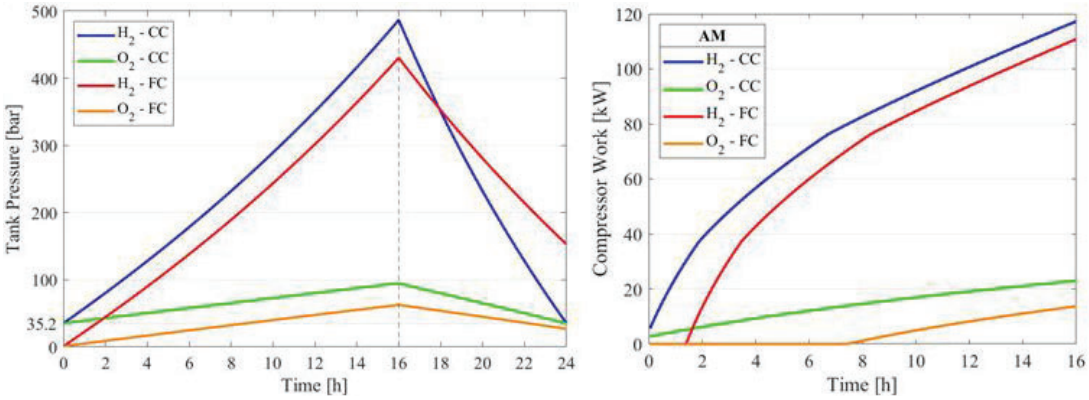

Figure 3: Tank Pressure (left, AM & BM) and Compressor Work (right, AM only) time histories in CC and PEMFC.

The performance data of the base power plant and the proposed power cycle in the different operation modes are summarized in Table 3. The excess energy produced by the BM-CC system compared to BPP amounts to 1395 kW, which is the same power rating assumed for the PEMFC in the BM. During accumulation, approximately 304 MWh of the net power is generated, with around 59 MWh consumed by auxiliaries. The AWE emerges as the predominant consumer among these auxiliaries, constituting 96.7% of the total auxiliary consumption. To maximize power output, the differences between the BM-CC and BM-FC options are minimal, with a marginal edge for the latter due to slightly lower auxiliary consumptions. The booster mode includes the additional energy contribution from hydrogen. Notably, BM-FC outperforms in efficiency and boasts a simpler plant arrangement compared to BM-CC.

The exergy analysis allows to compare different sources of irreversibility. Table 4 shows the relative exergy destruction for each component. For clarity, components with negligible calculated irreversibility (below 0.05%), such as pumps, compressors, coolers, vessels, etc., have been excluded from the table. Furthermore, the accumulation scenarios for both CC and FC cases were collectively represented as AMs, given their uniform outcomes.

The total exergy destruction within each system is 16.4 MW for BPP, 17.6 MW for AMs, 19.7 MW for BM-CC, and 18 MW for BM-FC. Notably, the component demonstrating the highest exergy destruction across all systems is, the low-pressure turbine (LPT). After the turbine, other noteworthy contributors to exergy destruction include the flash valve (FV) and the cooling tower (CT). Together, these three elements cover about 91.8% (BPP), 85.75% (AMs), 78.87% (BM-CC), and 83.67% (BM-FC) of the total exergy destruction. Breaking down these percentages further, the LPT contributes 35.8%, 33.4%,

https://doi.org/10.52202/077185-0123

31.4%, and 32.7% for BPP, AMs, BM-CC, and BM-FC. The Flash Valve contributes 34%, 31.8%, 28.5%, and 31%, while the Cooling Tower contributes 21.9%, 20.5%, 19%, and 20%. It's noteworthy that BM-CC exhibits an additional significant contribution from the combustion chamber (CC).

Table 3: Performance comparison of the base power plant and proposed power cycle modes.

Parameter	Item	BPP	AM (CC)	BM (CC)	AM (FC)	BM (FC)
Heat exchanged [kW]	Steam Condenser	71943	71943	75503	71943	71943
	Cooling Tower	77036	77036	80703	77036	77036
	Pre-Heater	/	42.31	/	42.31	/
	H_2 Coolers*	/	89	/	78.24	/
	O_2 Coolers *	/	22.9	/	11.93	/
	H_2 Vessel*	/	0.2267	/	0.4802	/
	O_2 Vessel*	/	0.05224	/	0.2449	/
Power [kW]	LP Turbine	22743	22743	23908	22743	22743
	Overall Pump	29.61	29.93	32.75	29.93	29.61
	AWE	/	3600	/	3600	/
	H_2 Compressors*	/	77.01	/	65.73	/
	O_2 Compressor*	/	14.04	/	3.999	/
	HP Turbine	/	/	229.7	/	/
	PEMFC	/	/	/	/	1395
Net Power		22713	19022	24105	19043	24108
First law efficiency [%]		22.77	21.54	23.03	21.57	24.89
Second law Efficiency [%]		58.04	55.07	55.04	55.09	57.46

* Average value

Table 4: Component exergy destruction comparison [%].

Study cases	Components													
	FV	LPT	SC	CT	M1	M2	AWE	CC	HPT	FC	V1	V2	M3	TOT
BPP	14.3	15.0	0.55	9.2	0.08	2.8	/	/	/	/	/	/	/	41.96
AMs	14.3	15.0	0.55	9.2	0.08	2.8	2.9	/	/	/	/	/	/	44.9
BM-CC	12.8	14.1	0.5	8.56	0.07	2.2	/	6.2	0.1	/	0.2	0.0	0.2	44.97
BM-FC	13.3	14.0	0.5	8.56	0.07	2.6	/	/	/	3.3	0.4	0.1	/	42.86

4.2 Exergo-Economic Analysis (EEA)

The first step of the EEA is to retrieve the PEC of the components (Table 5). For the BPP, the overall specific investment cost of the power plant is 3597 €/kW, which is in line with values common in GPPs (IRENA, 2023). The EEA directly yields the LCOE, which was calculated at 5.6 c€/kWh.

In the CC option, the overall specific investment cost of the power plant is 4113 €/kW, while for the PEMFC case, it is 4086 €/kW.

Figure 4 provides a comprehensive overview of the economic impact for each system. As is normal in GPP applications, the wells exhibit a high value of ($\dot{Z}_k + \dot{C}_{D,k}$) because of the considerable investment cost. The main turbine LPT is the second most relevant component. For the CC system, the combustion chamber is characterized by the large exergy destruction associated with the chemical reaction. In the FC model, the fuel cell emerges similarly with the highest economic impact, which is again dominated by exergy destruction due to electrochemical irreversibilities.

https://doi.org/10.52202/077185-0123

Table 5: Values of relevant exergo-economic variables.

k-th Component	BPP			BPP +Spinning Reserve (CC)			BPP +Spinning Reserve (FC)		
	PEC [€]	f_k [%]	r_k [-]	PEC [€]	f_k [%]	r_k [-]	PEC [€]	f_k [%]	r_k [-]
FV+Wells	4.9E+7	96.42	0.1218	4.9E+7	96.42	0.1218	4.9E+7	69.42	0.1218
SR	6670	100	0.0006	6670	100	0.0006	6670	100	0.0006
LPT	6.8E+6	76.14	1.0844	7.0E+6	35.89	0.5729	6.8E+6	76.14	1.0843
SC	344032	81.49	0.3271	354649	40.87	0.1626	344032	81.49	0.3272
CEP	28413	66.28	1.1778	28717	67.27	1.2863	28413	67.66	1.2943
CT	321087	15.03	3.8964	336080	6.12	3.4560	321087	15.05	3.8970
RMP	42058	35.32	0.6532	41701	38.85	0.7009	42058	37.64	0.6900
PH	/	/	/	368950	34.88	0.6709	357905	34.19	0.6214
EFP	/	/	/	20553	96.38	9.2050	20553	96.38	9.2050
AWE	/	/	/	2.8E+6	38.25	0.7047	2.8E+6	38.25	0.7047
H_2 Compressors	/	/	/	508497	89.95	2.7263	485719	91.09	3.2473
H_2 Coolers	/	/	/	195443	40.73	0.1185	136505	41.63	0.1047
H_2 Vessel	/	/	/	123012	99.97	0.0014	123012	99.93	0.0022
O_2 Compressor	/	/	/	120374	92.01	2.8260	92972	96.59	7.5250
O_2 Coolers	/	/	/	6846	22.04	0.0747	5181	31.81	0.0448
O_2 Vessel	/	/	/	328031	100	0.4497	328031	100	0.7085
CCFP	/	/	/	39089	87.13	2.9350	/	/	/
CC	/	/	/	3.4E+6	8.46	1.7350	/	/	/
HPT	/	/	/	1.2E+6	55.98	0.2547	/	/	/
FC	/	/	/	/	/	/	4.6E+6	6.79	1.173
Total Plant	**5.6E+7**			**6.6E+7**			**6.5E+7**		

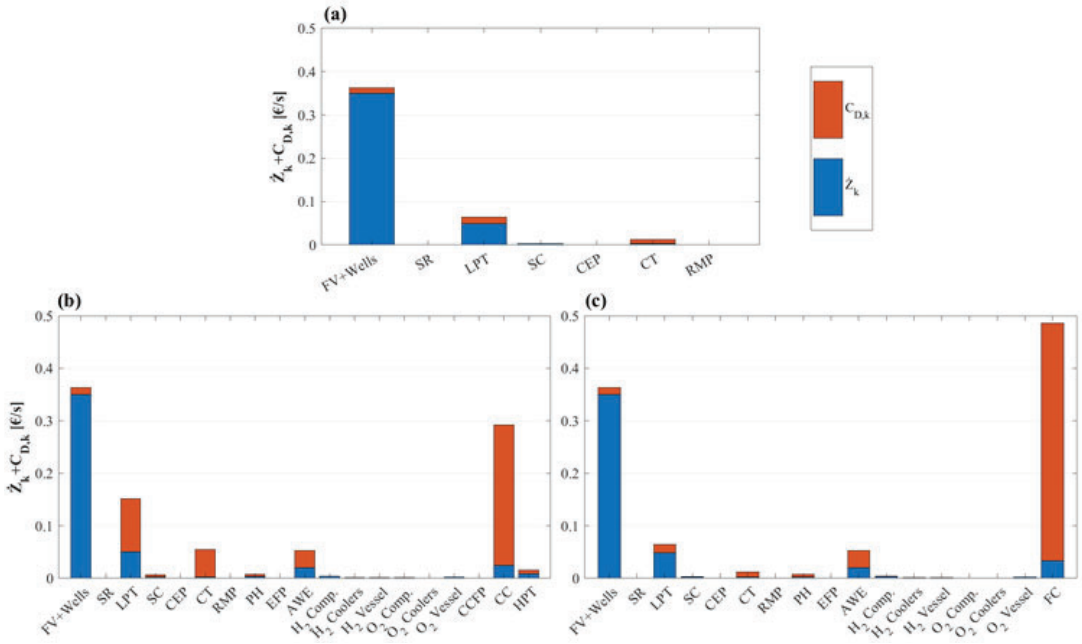

Figure 4: Economic impact (Capital Cost and Exergy Destruction) for each system: (a) BPP, (b) Modified BPP with CC, (c) Modified BPP with PEMFC.

https://doi.org/10.52202/077185-0123

4.3 Comparative electricity costs on typical days in May, June, July

In this section, the exergo-economic results for a typical day in the months under consideration (May, June, July) are presented. The cost of electricity was calculated by distributing costs based on operation hours in accumulation mode (AM) and booster mode (BM), which vary monthly. The specific exergy cost was also considered, varying with the operating mode.

Figure 5 illustrates the results, with dotted lines representing different operational modes, and solid lines representing the average electricity cost for each case study. The solid purple line represents the national electricity cost, while the grey line illustrates the trend of national PV contribution. Peaks in PV production coincide with lower electricity market prices, indicating a period of reduced profitability.

The electricity cost (EC) for each case study reflects the total cost of electricity production and, consequently, the minimum selling price required for economic competitiveness. Both system's minimum selling prices are lower than the national EC for each month, highlighting their advantageous position in terms of market competitiveness.

When the PV contribution is positive, depicted by the grey shaded area, it represents the AM, with costs delineated by dotted light green and dark green lines for CC and FC systems, respectively. These lines, although drawn for the entire 24-hour period, apply only to the grey shaded AM phase. Conversely, during the early hours and in the evening, when the PV contribution is zero, the system operates in power production mode (BM) within the white area of the graph. The costs in this mode are depicted by dotted purple lines for the combustion model and dotted red lines for the FC model, which are relevant exclusively during the white BM phase.

During AM, the electricity cost (EC) remains approximately constant for both study systems over time. This consistency arises from calculations based on the output of the low-pressure turbine (LPT), which is solely dependent on the constant cost of the geothermal resource. Conversely, during power production mode (BM), the EC fluctuates with the national electricity price. This cost, computed at both LPT and HPT outlets for the combustion system and at both LPT and PEMFC outlets for the FC system, varies depending on multiple points in the cycle, all influenced by the national electricity price. Generally, the CC system's EC in BM is comparable to, and in June even lower than, the national EC, while the FC system's EC is typically higher.

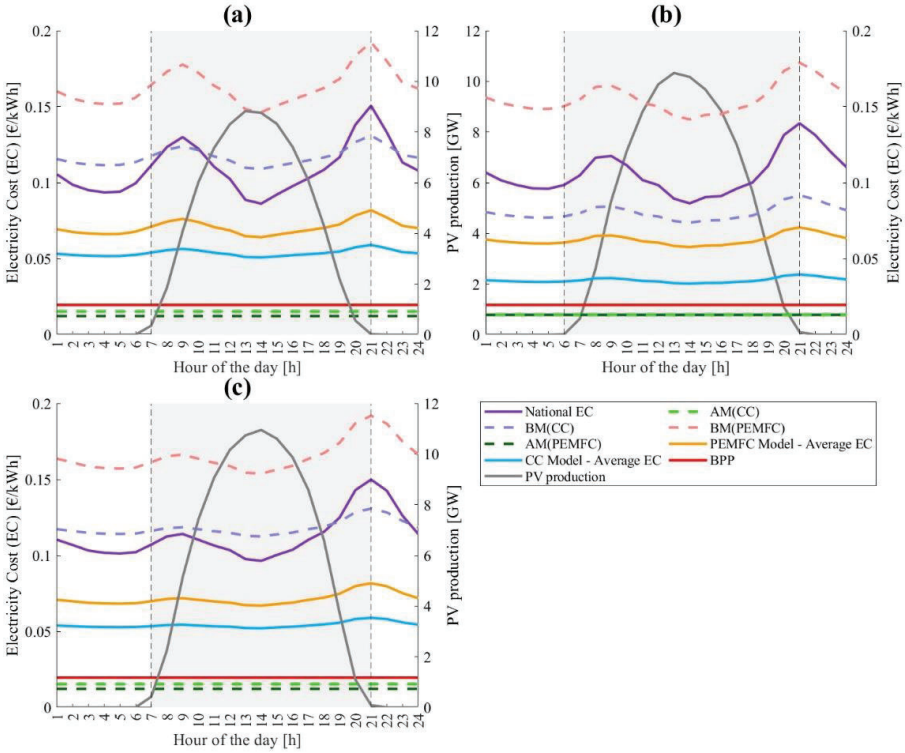

Figure 5: Variation of electricity cost with the working mode: (a) May, (b) June, (c) July.

https://doi.org/10.52202/077185-0123

5 CONCLUSIONS

The feasibility of integrating an electrolyzer and a H_2 spinning reserve into a single-flash geothermal power plant was explored to assess its economic viability in mitigating load variations associated with photovoltaic energy. The modified plant operates in two modes: hydrogen/oxygen storage and energy production. For each month from May to June 2023 in Italy, a typical day was analyzed, considering the national electricity price and the hourly contribution of national photovoltaic energy. The latter is pivotal in activating and deactivating each operational mode. Distinct thermodynamic and exergy models were developed for each mode, along with an exergo-economic model for the entire plant, providing a detailed overview of the economic and energetic performance of both systems. Both studied systems, CC and FC, exhibit comparable electricity production efficiency, albeit lower than the Base Power Plant (BPP) due to electrolyzer and rotating reserve implementation. Results indicate a potential load capacity increase in the Booster Mode (BM) of almost 1.4 MWe, which is retained compatible with marginal off-design operation of the 20 MWe nominal capacity of the power plant. The economic feasibility study yielded positive results, demonstrating that the CC system's electricity production costs in BM are comparable to or lower than the national electricity price, while the FC system's costs tend to be higher. This encouraging result suggests the system's potential to flatten photovoltaic load peaks while maintaining economic competitiveness. Additionally, the studied plant effectively attenuates photovoltaic load peaks, achieving a power difference of approximately 5 MW between the AM and BM operation modes. This is an important step in broadening the load flexibility of GPPs, which is one of the current goals of the sector SRIA. Considering that on the whole about 30 plants of this type (20 MWe capacity) are present in Italy (all of them currently in Tuscany), this represents a substantial equivalent storage and load flexibility capacity when scalability is considered. The plant's versatility allows for different operations during winter months when photovoltaic load peaks are less problematic. An unexplored positive aspect in this study is the system's ability to rapidly adjust production within seconds, making it highly suitable for electricity regulation on the grid. The study demonstrates that utilizing hydrogen as a rotating reserve presents a promising alternative to fossil fuel-based reserves, particularly when hydrogen is produced through geothermally-powered electrolysis, ensuring a fully renewable and environmentally friendly system.

NOMENCLATURE

$\dot{C}$	cost rate	(€/s)
c	cost per unit exergy (€/kJ or €/kWh)	
$\dot{E}x$	exergy	(kW)
h	enthalpy	(kJ/kg)
m	mass (kg)	
$\dot{m}$	mass flow rate	(kg/s)
p	pressure (kPa)	
s	entropy	(kJ/kgK)
T	temperature	(K)
y	exergy destruction ratio	(-)
$\dot{Z}$	capital cost rate	
ε	exergy efficiency	

Subscript

0	reference environment
D	destruction
F	fuel
i	initial
j	j-th stream
k	k-th component
L	loss
P	product
S	system

Acronyms

AM	Accumulation Mode
AWE	Alkaline Water Electrolyser
BM	Booster Mode
BPP	Base Power Plant
CC	Combustion Chamber
EC	Electricity Cost
EEA	Exergo-Economic Analysis
EES	Engineering Equation Solver
GPP	Geothermal Power Plant
PEC	Purchased Equipment Cost
PEMFC	Proton Exchange Membrane Fuel Cell
PV	Photovoltaic
SRIA	Strategic Research and Innovation Agenda
TCI	Total Capital Investment

https://doi.org/10.52202/077185-0123

REFERENCES

Bejan A., Tsatsaronis G., Moran M. J. (1996). *Thermal design and optimization*. John Wiley & Sons.

Campanari S., Guandalini G., Coolegem J., Ten Have J., Hayes P., Pichel A. H. (2019). Modeling, Development, and Testing of a 2 MW Polymeric Electrolyte Membrane Fuel Cell Plant Fueled with Hydrogen from a Chlor-Alkali Industry. *J. Electrochem. Energy Convers. Storage*, *16*(4).

DiPippo, R. (2012). *Geothermal Power Plants: Principles, Applications, Case Studies and Environmental Impact* (Third Ed.). Butterworth-Heinemann.

Dunikov, D. O. (2018). Cycle improvement and hydrogen steam superheating at Mutnovsky geothermal power plant. *Case Studies in Thermal Engineering*, *12*, 736–741.

Dunikov, D. O., Borzenko, V. I., & Schastlivtsev, A. I. (2022). Compact and fast-response 150 kW hydrogen-oxygen steam generator. *Int. J. Hydrogen Energy*, *47*(84), 35897–35902.

Fiaschi, D., Manfrida, G., Rogai, E., & Talluri, L. (2017). Exergoeconomic analysis and comparison between ORC and Kalina cycles to exploit low and medium-high temperature heat from two different geothermal sites. *Energy Conversion and Management*, *154*, 503–516. https://doi.org/10.1016/j.enconman.2017.11.034

Fuel Cells and Hydrogen Joint Undertaking (FCH JU). (2014). *Multi-Annual Work Plan 2014 - 2020.* https://ec.europa.eu/research/participants/data/ref/h2020/other/legal/jtis/fch-multi-workplan_en.pdf

IRENA (Int. Renew. Energy Agency). (2023). *RENEWABLE POWER GENERATION COSTS IN 2022*. www.irena.org

Klein, S., & Nellis, G. (2011). *Thermodynamics*. Cambridge University Press.

Kotas, T.J., The exergy method of thermal plant analysis, Krieger, 1995.

Lazzaretto, A., & Tsatsaronis, G. (2006). SPECO: A systematic and general methodology for calculating efficiencies and costs in thermal systems. *Energy*, *31*(8–9), 1257–1289. https://doi.org/10.1016/j.energy.2005.03.011

Malyshenko, S. P., Gryaznov, A. N., & Filatov, N. I. (2004). High-pressure H2/O2-steam generators and their possible applications. *International Journal of Hydrogen Energy*, *29*(6), 589–596.

Manfrida, G., Talluri, L., Ungar, P., Zuffi, C., Díaz-Ramírez, M., Leiva, H., Mainar-Toledo, M. D., & Jokull, S. (2023). Exergo-economic and exergo-environmental assessment of two large CHP geothermal power plants. *Geothermics*, *113*. https://doi.org/10.1016/j.geothermics.2023.102758

Meyer, L., Tsatsaronis, G., Buchgeister, J., & Schebek, L. (2009). Exergoenvironmental analysis for evaluation of the environmental impact of energy conversion systems. *Energy*, *34*(1), 75–89.

Schuster, A., Karellas, S., Kakaras, E., & Spliethoff, H. (2009). Energetic and economic investigation of Organic Rankine Cycle applications. *Applied Thermal Engineering*, *29*(8–9), 1809–1817.

Shokati, N., Ranjbar, F., & Yari, M. (2015). Exergoeconomic analysis and optimization of basic, dual-pressure and dual-fluid ORCs and Kalina geothermal power plants: A comparative study. *Renewable Energy*, *83*, 527–542. https://doi.org/10.1016/j.renene.2015.04.069

Stathopoulos, P., Sleem, T., & Paschereit, C. O. (2017). Steam generation with stoichiometric combustion of H2/O2 as a way to simultaneously provide primary control reserve and energy storage. *Applied Energy*, *205*, 692–702. https://doi.org/10.1016/j.apenergy.2017.07.094

Sternfeld H. J. (1995). *Capacity control of power stations by O2/H2 rocket combustor technology*. *37*.

Turton, Richard, Bailie, Richard C, Whiting, Wallace B, Shaeiwitz, & Joseph A. (2017). *Analysis, Synthesis and Design of Chemical Processes.* (5th Ed.). Prentice-Hall.

ACKNOWLEDGEMENT

This research was supported within the frame of the Italian National Recovery and Resilience Plan (NRRP), Mission 4, Component 2 Investment 1.3 - Call for tender No. 1561 of 11.10.2022 by Ministero dell'Università e della Ricerca (MUR); funded by the European Union – NextGenerationEU Project code PE0000021, MUR Concession Decree No. 1561, CUP - I53C22001450006, Project title "Network 4 Energy Sustainable Transition – NEST"

https://doi.org/10.52202/077185-0123